

A Microservices-based Framework for Smart Design and Optimization of PV Installations

Original

A Microservices-based Framework for Smart Design and Optimization of PV Installations / Vinco, Sara; Jahier Pagliari, Daniele; Bottaccioli, Lorenzo; Patti, Edoardo; Macii, Enrico; Poncino, Massimo. - In: IEEE TRANSACTIONS ON SUSTAINABLE COMPUTING. - ISSN 2377-3782. - 6:4(2021), pp. 531-543. [10.1109/TSUSC.2020.3010673]

Availability:

This version is available at: 11583/2841229 since: 2021-12-09T10:17:10Z

Publisher:

IEEE

Published

DOI:10.1109/TSUSC.2020.3010673

Terms of use:

This article is made available under terms and conditions as specified in the corresponding bibliographic description in the repository

Publisher copyright

IEEE postprint/Author's Accepted Manuscript

©2021 IEEE. Personal use of this material is permitted. Permission from IEEE must be obtained for all other uses, in any current or future media, including reprinting/republishing this material for advertising or promotional purposes, creating new collecting works, for resale or lists, or reuse of any copyrighted component of this work in other works.

(Article begins on next page)

A Microservices-based Framework for Smart Design and Optimization of PV Installations

Sara Vinco, *Member, IEEE*, Daniele Jahier Pagliari, *Member, IEEE*, Lorenzo Bottaccioli, *Member, IEEE*, Edoardo Patti, *Member, IEEE*, Enrico Macii, *Fellow, IEEE* and Massimo Poncino, *Fellow, IEEE*

Abstract—The design of photovoltaic (PV) installations mostly relies on rule-of-thumb criteria and on gross estimates of the shading patterns, and the few optimized approaches are generally focused on the problem of identifying the most suitable surfaces (e.g., roofs) in a larger geographic area (e.g., city or district).

This work proposes a framework to address the design and the optimization of PV installations through a set of microservices focusing on the different variables of the design: identification of the target surfaces, elaboration of weather data, modeling of the PV panel, and floorplanning of the panel on the surface. The microservices architecture ensures extensibility and generality, as the user may execute only a subset of the proposed services or provide novel algorithms to extend the existing ones. Additionally, the framework provides a set of built-in models that allow sensitivity to the distribution of shades and accurate modeling of the power production over time. We show the many benefits of the proposed framework on two different use cases.

Index Terms—Photovoltaic installation, renewable energy, microservices, PV design, PV optimization, GIS-based design.

1 INTRODUCTION

Environmental sensitivity is progressively bringing towards the replacement of energy generation based on fossil fuels with renewable energy sources. Although not the largest contributor to renewable energy, the share of solar energy is constantly growing due to several strengths of photovoltaic (PV) installations, namely, decreasing costs, scalability, easy deployment, limited invasiveness in existing infrastructures, and economic incentives [1].

When deploying PV installations for large-scale solar farms, the determination of the cost-optimal location for the installation is the key design decision [2]–[7]. However, in other scenarios [8]–[12], such as residential or industrial installations, the location is in most cases pre-defined (e.g., a portion of a given roof), and other issues such as the impact of transient shadings or of the quality of the chosen PV modules on total cost have a higher impact for the user [13]. Additionally, recent works [14]–[16] highlighted the importance of the actual placement of modules on the target surface: by exploiting fine-grain irradiance data, obtained by meteorological and GIS-based sources, the energy output of a PV installation can be significantly increased by relaxing the traditional compact floorplanning of PV installations to allow individual placement of PV modules so to optimally match irradiance conditions [15], [16].

It is therefore useful to have a single tool able to evaluate the impact of multiple variables (type of PV module, granularity of environmental data, characteristics of the target surface,

and floorplanning options) on the power/energy output and on the installation cost. Some simulation frameworks with this objective do exist [1], [8], [17]–[19], but they either focus only on some of these variables, or they do not easily allow to perform design space exploration.

In this work we propose a framework for the evaluation of residential or industrial PV installations that overcomes the limitations of previous methods. The framework is organized as a microservices architecture, i.e., *as a suite of small services, each running in its own process* [20] and covers all phases of the design of a PV installation, e.g., the identification of the suitable area on the roof of interest, the choice of the PV modules, and the placement of the PV modules on the roof.

The key features of the proposed framework are:

- **Modularity and generality:** Our framework allows to define multiple scenarios *by using either all or only some of the defined microservices*. Similarly, it allows the reuse of existing models or data: e.g., it is possible to provide user-defined PV power models, or to reuse pre-existing irradiance traces. This is made possible by the microservices architecture, which allows to replace the execution of some services with existing pre-processed data, with the only constraint of complying to the microservice interface. This is in clear contrast with existing frameworks that usually assume a specific module type, panel architecture, or time granularity of the input traces; changing those usually requires significant changes to the framework.
- **Variable accuracy:** A consequence of the previous item is that the level of detail of models and data is not pre-defined. Both can be made more or less accurate to emphasize one particular feature over another. For instance, some details about the PV model can be neglected to speed up the exploration of the different placements.

• S. Vinco, D. Jahier Pagliari, L. Bottaccioli, E. Patti and M. Poncino are with the Department of Control and Computer Engineering, Politecnico di Torino, Turin, Italy (e-mail: {name.surname}@polito.it). E. Macii is with the Interuniversity Department of Regional and Urban Studies and Planning, Politecnico di Torino, Turin, Italy (e-mail: {name.surname}@polito.it).

Manuscript received xxxxx; revised xxxxx.

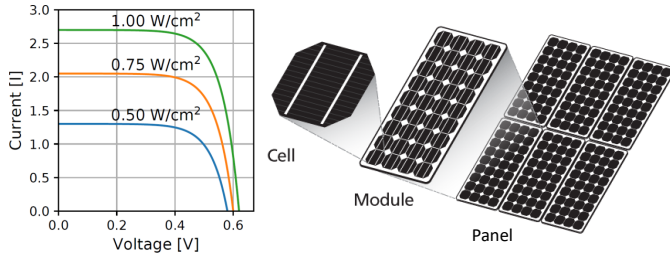


Fig. 1. I-V curve (left) and PV components hierarchy (right).

- **Design space exploration:** Another consequence is that, since every model, option, and datum may be user-specified, an exhaustive design space exploration can be run to analyze the power output of a PV installation for different values of all key parameters.

The manuscript is organized as follows: Section 2 provides some background and reviews the related state of the art. Section 3 introduces the proposed framework, whose constituting modules are described in Sections 4-9. Section 10 applies the proposed approach to two use cases. Section 11 concludes the paper.

2 BACKGROUND AND RELATED WORK

2.1 PV Component Hierarchy

The basic element of a photovoltaic generator is the cell, whose electrical behaviour can be described by an ideal current source, proportional to solar irradiance, and a diode connected in anti-parallel. A cell is described by a voltage-current (I-V) characteristic curve, for a given cell temperature T and irradiance G (left-hand side of Figure 1). The open-circuit voltage V_{oc} increases logarithmically and the short-circuit current I_{sc} increases proportionally for increasing G . Under a given G , an increase of T yields a slight increase of the I_{sc} which in turn gives a decrease of V_{oc} . Cells are then series-connected to form a PV *module* to achieve voltages of a few tens of volts (typical modules consist of 36–72 series-connected cells). PV modules are then further interconnected to form a PV *panel*, this time in a series/parallel combination to achieve the desired output voltage and current levels (right-hand side of Figure 1).

Defects or shading can result in non-uniform irradiance in the cells of a module, thus affecting the total output power. Because of the different power levels, a Maximum Power Point Tracker (MPPT) is used to extract the maximum available power and to maximize the efficiency [21].

2.2 Geographic Information Systems

Geographic Information Systems (GIS) are often exploited to model solar potential and to plan the deployment of solar generators [22]. The starting point is usually a *Digital Surface Model* (DSM) or a 3D city model obtained from LiDAR data, representing terrain and building elevation of an area. Mapwell Solar System [23] and i-Guess [24] provide information on solar radiation and PV potential, but they are limited to yearly estimations only. I-SCOPE [25] is an integrated platform that offers a solar map with yearly and monthly PV potential. The above solutions suffer from many limitations. Sub-hourly information is necessary to better

estimate the optimal energy production, and coarse resolutions (i.e., $> 1m$) do not allow to recognize obstacles on rooftops (e.g., chimneys, dormers). Moreover, real weather data from weather stations must be considered to provide accurate estimations.

2.3 Related work

Efficient PV design and installation has been deeply investigated in the literature, with works that focus on different aspects of the problem, ranging from weather trace generation to identifying suitable geographic areas and estimating the correct sizing of the necessary energy storage devices (i.e., batteries).

Table 1 reports the most relevant works recently proposed: as the Table highlights, a major limitation is that all works focus on a single aspect of PV design, while other aspects are either supported with simplistic models or considered as input configuration. Note that, due to space constraints, the table can not be exhaustive: we had to choose representative works for each perspective on the design flow.

The solutions in [26]–[29] [30] work with refined geographic and shadow data, but they abstract the modeling of PV power production, both in terms of models and of accuracy w.r.t. the actual topology and physical position of the modules. Other approaches focus on the optimal sizing of the PV installation [2], [9], [31]–[33], on the identification of optimal management algorithms [17], [18] or on the optimal roof configuration (e.g., tilt angle) [34] [4], [35], [36], by abstracting on the other aspects of PV designs. Vice versa, the works in [3], [8], [19], [27]–[29] [5] focus on the identification of suitable areas at large (i.e., entire roofs or geographical areas), with no detailed information about the actual placement of PV modules and with very abstract models of PV power production. Finally, a number of models of PV modules have been proposed in the literature, with different levels of accuracy w.r.t. the intrinsic dynamics of PV power generation and to the connection topology [37]–[41] [42]; however, these works restrict the focus on the sole modeling, with no support for the other aspects of PV design.

Interestingly, most of the approaches available at state of the art (despite of [27]–[29]) provide monolithic software implementations, that can not be easily extended or integrated with other software.

From the Table, it is thus evident that optimal PV design can be achieved only by adopting a number of tools, each focusing on a specific aspect, with possibly conflicting output solutions. The designer is thus forced to choose a specific view of the problem and to prefer a certain dimension at the expense of the others, thus achieving sub-optimal outcome and limiting the space of exploration.

This work (bottom of Table 1) proposes to overcome the limitations of the current state of the art by providing a holistic framework that addresses all the issues involved in the design of a PV installation. Additionally, the proposed framework is built as a set of microservices, thus enhancing modularity, future extensibility and integration with other tools.

TABLE 1
Overview of representative related works on PV design

REF.	WEATHER DATA MANAGEMENT	SHADOW MODEL	PV MODULE MODEL	PV PLACEMENT	PV SIZING	SOFTWARE ARCHITECTURE
[17], [18]	High resolution (1 minute to 1 second)	Shadows only as scaling pattern [17] or over-estimated [18]	Circuit model [17]; not presented for [18]	Fixed	Fixed; optimize maximum power point (MPP) algorithm	Monolithic
[3], [8], [19] [5]	Variable irradiance accuracy (yearly [3], [19] to hourly [8] [5]); no temperature data	Delegated to other tool [3], [19] or absent [8]	Simple equation model based on rated power, area and derating factors	Determines optimal roof for PV installation, [5] identify best areas w.r.t. land cover, and distance from the electricity grid	Determine optimal sizing to maximize profit [8], [19] or to estimate the occupied area	Monolithic
[26]	1 year of real data from weather stations (hourly granularity, uniform over the area of interest)	Refined with small spatial granularity	Circuit model of PV cells with diodes support; requires measurements	Fixed	Fixed	Monolithic
[27]–[29], [30], [36]	Typical hourly weather traces	None [28] or with low spatial resolution [27], [29] [36]	Power as linear function of temperature and irradiance, [36] uses [28]	Returns information on rooftops [28] or larger areas [29], [30] identify suitable areas from aerial photo, [36] optimize orientation w.r.t. low volatility and grid stability	Fixed	Monolithic
[2], [9], [31]	1 year trace with 30 minutes (or longer) [31], hourly [9], or 5-minutes [2] resolution; uniform over the area of interest	None	Simple linear equation models ([31] no shading; [9] scales 1 PV module to N PV modules; [2] power as function of area)	No information about placement and connection of PV modules	Determines optimal sizing of PV modules and battery to minimize requests to the grid	Monolithic
[32], [33]	Statistical monthly irradiance	None	Commercial software	Fixed	Cost analysis and sizing of batteries and inverter	Commercial software
[34]	10 years of monthly average weather data	None	Linear equation based on average energy conversion efficiency	Fixed (focuses on occupied m^2)	Optimize surface tilt angle and array size, not the actual placement	Monolithic
[4]	Direct and Diffuse solar measurements	[27]	Linear equation based on average energy conversion efficiency	Fixed (focuses on occupied m^2)	Optimize surface tilt angle and array size on flat roof-top	Monolithic
[35]	Daily and monthly values	None	Linear equation based on average energy conversion efficiency	Fixed (focuses on occupied m^2)	Optimize surface tilt angle and orientation	Monolithic
[43]	Real weather traces from a reference 1kW PV system with corresponding power production	None	Trains 11 prediction models with corresponding PV production	Fixed	Fixed	Monolithic
[37]–[41] [42]	None	None, sensitive only to irradiance values	Different accuracy levels: from circuit-level [37], [38] to interpolation derived from datasheet information [39] [42]	Fixed; sensitive to different connections	Fixed	Monolithic
This work	High resolution irradiance and temperature traces: 15 minutes, 20x20cm (<i>Trace Builder</i>)	Based on GRASS-GIS with generation of radiation maps (<i>Trace Builder</i>)	Equation based on datasheet (no measurements); supports presence of diodes and multiple topologies (<i>PV Module and PV Panel Model Builder, Simulator</i>)	Compact or heuristic irradiance-based placement of PV modules on roof of interest (<i>Placement Configurator</i>)	Supported, based on monetary budget or desired power levels (<i>Topology Builder</i>)	Microservices

3 PROPOSED FLOW

Figure 2 shows the flow of the proposed PV design software infrastructure, which consists of six different blocks.

The inputs are shown on the left side of the flow and include:

- The meteorological data obtained from weather stations, namely irradiance (i.e., Global Horizontal Irradiance $GHI(t)$) and ambient temperature over time.
- A DSM of the buildings of interest.
- The cadastral maps of the urban area of interest.
- The target output power, voltage and monetary budget of the overall panel.
- The specifications of the target PV module.

The first block is the **Trace Builder** (①): given the roof of interest, plus the DSM model and the cadastral maps, the Trace Builder derives the evolution of shadows on the roof over time. This shadow model is used then to tune the input environmental data to derive spatio-temporal traces of irradiance G and temperature T with a fine-grain spatial resolution. Both spatial and temporal resolution are user-configurable; in this work, we use a granularity of 15 minutes and $20\text{cm} \times 20\text{cm}$ tiles. This block also provides information on the suitable area, i.e., the real surface available on rooftops where PV modules can be deployed. The details are discussed in Section 4.

The **Topology Builder** (②) determines the required number of modules in the PV panel (N) and their series/parallel ($s \times p$) electrical interconnection, based on user-defined constraints on the desired output voltage and power, or on the available monetary budget. The details are discussed in Section 5.

The PV module specifications are used by the **PV module model Builder** (③) to build the model of an individual PV module, as described in Section 6. Its output is a function that yields a power value for a given value of G and T .

The block **PV panel model Builder** (④) uses the topology information (N, s, p) and the model of an individual PV module to assemble a model of the whole PV panel, as described in Section 7.

The **Placement Configurator** block (⑤) contains the algorithms for placing the PV modules on the suitable areas, together with their connections. The built-in algorithms provided by the Placement Configurator are described in Section 8, and include a standard “compact” placement, and an irradiance-driven placement.

The resulting placement, the PV panel model and the G and T traces are then given in input to the **Power Production Estimator** block (⑥), to obtain the resulting output power waveform (Section 9).

The proposed software infrastructure has been designed following the microservices design pattern, which makes it distributed and modular. In the microservices approach, software is developed as a suite of small services, each running in its own process and communicating with lightweight mechanisms [20], [44]. Compared to current solutions that are monolithic, microservices increase software flexibility and maintainability because services are small, highly decoupled and focus on doing a small task. Additionally, this approach eases the integration of our solution with third-party software and fosters the development of new services.

In the proposed infrastructure, all blocks expose REST Web Services [45] and can be executed sequentially, given the input data up to the generation of output power waveforms. The user may customize some of the blocks, to evaluate different options e.g., a different model for PV modules to emphasize different characteristics, or a different placement algorithm. In alternative, the user may run only part of the flow, e.g., by replacing execution of some blocks with custom configurations, e.g., use pre-generated G and T traces. Notice that each microservice can be even invoked by third-party software.

The modularity of the microservices approach also enables the usage of part of the proposed infrastructure with legacy (pre-installed) PV systems, for example to estimate their power production over a given time span or to design upgrades (e.g. the addition of a new series string to an already placed panel). In the first scenario, the *Topology Builder* and the *Placement Configurator* would be clearly disabled, as the topology and placement of a legacy system are fixed. For the addition of new modules, instead, only the former would be disabled, as the topology of the new portion of panel must match that of existing modules; the *Placement Configurator*, instead, could be used to optimize the position of the newly added modules, simply removing the space occupied by the legacy system when determining the suitable placement area. In both scenarios, however, all the other microservices of Figure 2 would still be fully utilized.

4 TRACE BUILDER

The *Trace Builder* block consists of four distributed software components as shown in Figure 3. The full details on the approach to exploit geographic information to support PV design have been proposed by [46]. This section outlines the main steps of data processing and generation.

The **Clear-sky Conditions** component simulates solar radiation and shadows evolution in urban contexts by exploiting GRASS-GIS [47]. Due to the integration of high-resolution DSM the **Clear-sky Conditions** component is capable of simulating shadowing effects of small obstacles such as chimneys or dormers present in the rooftop. The inclination and the orientation (in degrees) of each pixel in the DSM are extracted, and from these direct and diffuse solar radiation maps in clear-sky condition with 15 minutes time interval are extracted. From these information, the **Suitable Surface** component identifies the surface where PV modules can be deployed, by excluding encumbrances, such as dormers, chimneys, or too small areas. The output is clipped with the cadastral map to produce a GeoJSON reporting a number of polygons representing the suitable area. The suitable area is additionally aligned with a virtual grid, whose elements have size equal to the granularity of the environmental traces (e.g., $20\text{cm} \times 20\text{cm}$), chosen so that it is a divisor of the sizes of a PV module. This builds a matrix where cells suitable to host a PV module are encoded with “1” the others (e.g., occupied by obstacles) with “0”. An example is provided on the left-hand side of Figure 4. The suitable area is then saved to a JSON file, used in the next steps of the flow.

The **Solar Radiation Decomposition** component retrieves meteorological information from third-party weather sta-

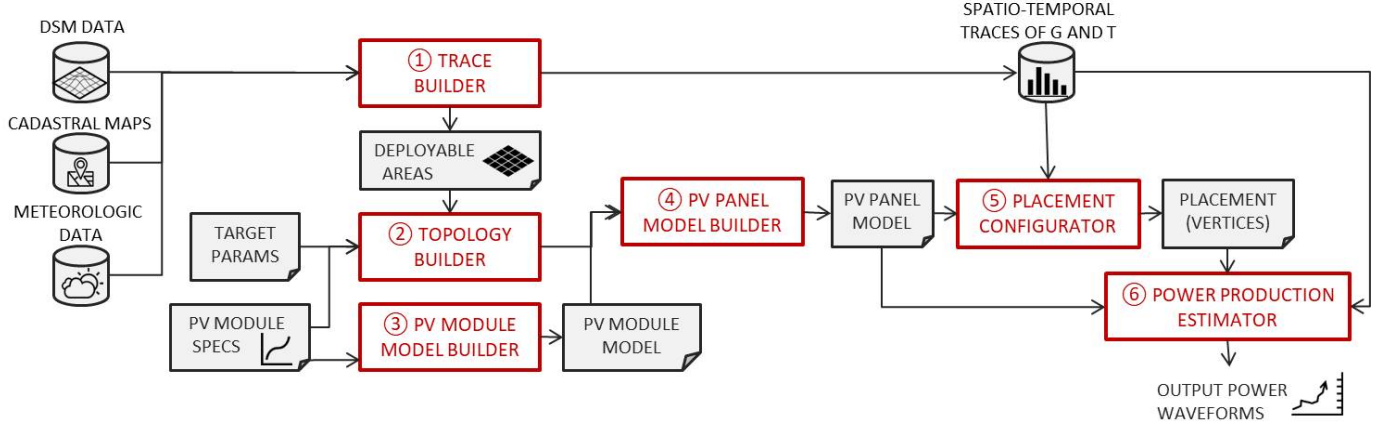


Fig. 2. Flow of the Proposed Framework for Smart Design and Optimization of PV Installations.

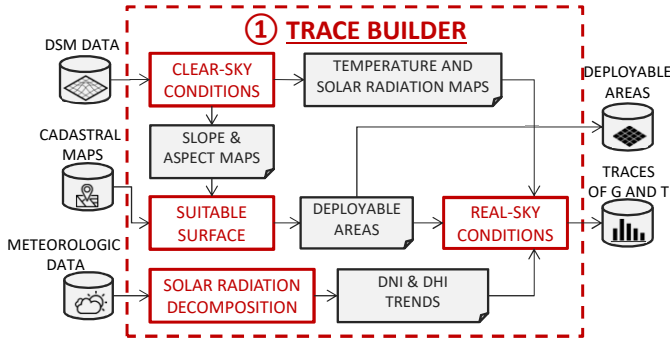


Fig. 3. Flow of the Trace Builder block.

tions to decompose the GHI into Direct Normal Irradiance (DNI) and Diffuse Horizontal Irradiance (DHI), according to one of six available decomposition techniques (e.g., [48]) that can be selected by end-users according to latitude, longitude and environmental conditions of the area of interest. The output is a JSON with the resulting values of DNI and DHI for a required time interval.

The **Real-sky Conditions** component simulates real-sky conditions providing a set of maps (as GeoTIFF images) of incident irradiance G onto the deployable areas for each time interval. To achieve this, it uses the DNI and DHI trends, the direct and diffuse solar radiation maps, and the suitable area. The component additionally builds a set of maps of ambient temperature on the irradiated roof surface T_{solair} , that is an accurate bias for the operating cell temperature [49]. T_{solair} is derived from ambient temperature T (from the meteorologic data) and from irradiance G as:

$$T_{solair}(G) = T + k \cdot G \quad (1)$$

where $k = 0.05 \frac{W}{K \cdot m^2}$ is the ratio of the absorptance of the roof divided by its radiative loss factor [49].

With respect to state-of-the-art solution for simulating solar radiation, this block provides the following capabilities:

- jointly analysing spatial and temporal domain with fine-grained resolution;
- providing real-sky sub-hourly simulations, with 15-minutes time intervals, essential to get accurate estimations of PV power generation;
- automatically identifying suitable surfaces for PV system deployment;

- integrating real meteorological data gathered from (personal) weather stations.

5 TOPOLOGY BUILDER

The *Topology Builder* determines the number of PV modules in each series string (s) and number of parallel strings (p) in the panel. In state-of-the-art frameworks, this information is usually determined by the user, or pre-defined by the framework constraints e.g., through ILP programming. Our framework allows the user to derive a possible topology given the target voltage V_{rated} , plus at least one out of two user-defined constraints: the target power P_{rated} to be extracted from the panel in nominal conditions, or a maximum cost budget for the installation C_{max} . This allows to explore different configurations and to evaluate different design constraints before actually realizing the PV installation.

5.1 Topology selection based on rated power

The number of modules s in a string is determined based on V_{rated} . Given the electrical characteristics of the module in rated conditions ($1000W/m^2$ and 25°) given by the PV module specs, the output voltage of the panel is equal to the voltage of a generic series string, i.e., $s \cdot V_{values,rated}$, where $V_{values,rated}$ is the rated value from the specifications. The value of s is obtained as:

$$s = \left\lceil \frac{V_{panel}}{V_{values,rated}} \right\rceil \quad (2)$$

where the ceiling operator is used to obtain an integer value for s . With similar considerations, the rated power of the panel can be computed as:

$$P_{rated} = s \cdot p \cdot P_{values,rated} = N \cdot P_{values,rated} \quad (3)$$

The value for $P_{values,rated}$ can be derived from the module specifications (assuming MPP tracking), which yields:

$$N = \left\lceil \frac{P_{rated}}{P_{values,rated}} \right\rceil, p = \left\lceil \frac{P_{rated}}{s \cdot P_{values,rated}} \right\rceil \quad (4)$$

5.2 Topology selection based on monetary budget

The value of s is determined using (2), as in Section 5.1. Next, a simple total cost model is used to determine N :

$$C_{tot} = N \cdot P_{values,rated} \cdot (C_{cap} + C_{om}) \quad (5)$$

where C_{cap} is the capital cost for one panel, including installation costs, and C_{om} is the operation and maintenance cost. Both are normally expressed in $\$/KW$, hence they depend on $P_{values, rated}$. We use $C_{cap} = 6500\$/KW$ and $C_{om} = 65\$/KW$ as defaults [50], but these values can be customized by the user.

The value of p is then determined as:

$$p = \left\lfloor \frac{C_{max}}{s \cdot P_{values, rated} \cdot (C_{cap} + C_{om})} \right\rfloor \quad (6)$$

where, being C_{max} an upper bound, the floor operator is used on p .

5.3 Feasibility Check

Placing the desired N modules on the roof may be physically impossible due to lack of space. To verify this occurrence, the topology builder performs a placement feasibility check, accounting for the obstacles described in the roof specification. Checking if N rectangular modules can be placed on an irregular surface is a variant of a two-dimensional bin packing and is therefore NP-Hard; therefore, to avoid increasing complexity too much, we perform a conservative check with a greedy heuristic, whose complexity is linear in the number of roof cells.

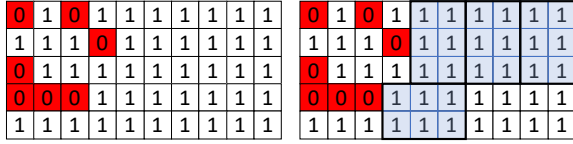


Fig. 4. Suitable area (left) and result of a topology feasibility check for $N = 4$ (right). Light blue rectangles represent placed modules.

Starting from the top-left corner of the suitable surface matrix, we greedily place the first PV module in portrait orientation as soon as a feasible location is found (i.e., a rectangle of “1”s that can host the PV module area). We then continue to place modules moving through the matrix column-first, until we reach the bottom-right corner. If there are still modules to be placed, we restart from the top-left considering a landscape orientation. Figure 4 shows an example with $N = 4$, in which a module occupies a 2×3 area. The overall time complexity of this service is $O(H \cdot W)$ where H and W are the height and width of the suitable area matrix, since each placement position is considered at most twice (one for each orientation).

If less than N modules have been placed at the end of this procedure, the tool assumes that the placement is unfeasible and raises an exception. Although this method may not be able to find the most compact placement overall, the missed solutions would have contained so tightly packed modules that their installation would be prohibitively complex. In contrast, finding a solution guarantees that the placement is indeed feasible.

6 PV MODULE MODEL BUILDER

This component builds the power model of an individual PV module. The inputs are the typical datasheet curves, i.e., (1) the I-V curve for different G values, and the dependence

of V_{oc} and I_{sc} on (2) cell temperature, and (3) on irradiance. As an example, Figure 5 shows these inputs for the Mit-subishi’s PV-MF165EB3 PV module, as extracted from the datasheet [51].

The only strictly necessary curve is the I-V one; if the other two curves not provided, V_{oc} and I_{sc} are assumed as independent of G and T , with obvious losses in accuracy. To allow automatic model construction, this information is digitized as JSON documents that describe each curve as its x-axis and y-axis quantities, any parameter (e.g., the corresponding G value), and a list of samples.

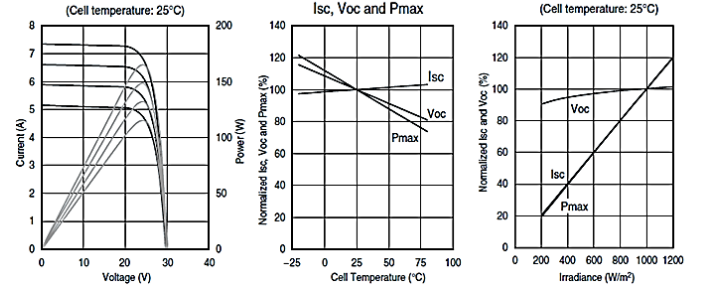


Fig. 5. Datasheet graphs for Mitsubishi’s PV-MF165EB3 PV module [51].

The output is a JSON document describing a function that, taken in input G and roof surface temperature T_{solair} , determines the corresponding I-V curve as samples of V and I .

The framework provides one built-in module model, which is a compact semi-empirical model built from information extracted from the datasheet [52]. The selection of this kind of model for the framework is a key aspect and an important plus, as the user can easily create a model for any PV module of interest, given only public information. This enables exploration: it is indeed possible to compare different PV modules with an accurate estimation of their dynamics. It is nonetheless important to note that the user may replace this model with any model at her complete discretion, by bypassing the execution of this block of the framework, or by extending the framework implementation with a new microservice following a different model.

The model of a PV module is built as follows. The temperature of a cell T_c is derived by using the relation between T_c and T_{solair} described in [53], that correlates with G and with characteristic coefficients of the PV module, such as its temperature coefficient and the transmittance of its cover.

As a next step, the model derives the dependence of V_{oc} and I_{sc} on G and T_c from the curves in the center and right plot of Figure 5, by empirically fitting the curves to obtain the coefficients for equations 7-8:

$$V_{OC}(G, T_c) = V_{OC, nom} (c_1 T_c + c_2) \cdot (c_3 G^{c_4} + c_5) \quad (7)$$

$$I_{SC}(G, T_c) = \alpha \cdot I_{SC, nom} (c_6 T_c + c_7) \cdot (c_8 G - c_9) \quad (8)$$

where $V_{OC, nom}$ and $I_{SC, nom}$ are the nominal V_{OC} and I_{SC} , c_i are coefficients obtained through curve fitting, and α is an aging factor (on average, 0.4%-1%/year) [54]).

The last step is to derive a function describing the I-V curve for different values of G . Since the PV cell is a diode, we use the generic equation of the I-V characteristic of an ideal

diode as a template to be fitted empirically to model the PV behavior:

$$I = I_{SC} - a \cdot (e^{b \cdot V} - 1) \quad (9)$$

where b is derived by imposing that $I(V_{oc}) = 0$:

$$b = V_{OC}^{-1} \cdot \ln(1 + I_{SC} \cdot a^{-1}) \quad (10)$$

Parameter a represents a measure of the curvature of the I-V curve and is a bias for the internal resistances of the PV phenomena (larger values of a will “flatten” the curve). The value of a is obtained through curve fitting from one I-V curves available in the datasheets (left of Figure 5).

Figure 6 shows the customization for the Mitsubishi's PV-MF165EB3 PV module from the specifications in Figure 5.

$$\begin{aligned} I_{SC} &= 0.93 \cdot I_{SC,nom} \cdot \frac{(0.55 \cdot T_c(T_{solair}, G) + 988.5)}{1000} \\ &\quad \cdot \frac{0.99 \cdot G^{-0.02} + 362.2}{1000} \\ a &= +4.428e^{-05} \\ b &= \frac{1}{V_{OC}} \cdot \log\left(1 + \frac{I_{SC}}{a}\right) \\ V &= [0 : 0.1 : V_{max}] \\ I &= I_{SC} - a \cdot (e^{b \cdot V} - 1) \end{aligned}$$

Fig. 6. Equations 7-10 fit to model a Mitsubishi's PV-MF165EB3 PV module from the datasheet data reported in Figure 5.

7 PV PANEL MODEL BUILDER

This component is in charge of building the power model of a panel consisting of an interconnection of PV modules according to a $s \times p$ interconnection, by using the PV power modules described in Section 6. This component allows maximum flexibility, in terms of topology, series/parallel combination and presence of bypass diodes. The configuration provided by the user or derived by the *Topology Builder* is automatically applied to model the connection of single PV modules by manipulating their equations with the following strategies. For the sake of readability, in the following we assume that the $s \times p$ interconnection consists of p parallel strings each with s modules in series; the description can be straightforwardly generalized to other topologies (e.g., a series of s clusters each with p modules in parallel).

7.1 Connecting PV modules

One important variable in this step is the possible presence of *bypass diodes*, that are typically placed across groups of series-connected cells or entire PV modules for bypassing shaded cells or modules, which would otherwise be limiting the output power of a series string. The distribution of bypass diodes has a heavy impact on power estimation [55]. This component takes in input a parameter d that indicates the number of diodes in the installation with the following meaning:

- $d = 0$: no diode is present between PV modules (diodes may be embedded inside of each PV module) [56];

- $0 < d \leq N$: a diode every d modules (with $N \% d = 0$).

The value of d leads to two different strategies to determine the result of connecting in series or in parallel strings or PV modules, as explained in the next sections.

7.1.1 Connection without bypass diodes

In absence of bypass diodes (i.e., $d = 0$), in a series-connected string, the PV module with the lowest current (i.e., irradiance) acts as a bottleneck and limits the current of the other PV modules. Similarly, for a parallel connection, the PV string with the lowest voltage constraints the voltage also of the other strings. The total power of the PV panel is thus obtained as $P_{panel} = V_{panel} \cdot I_{panel}$, where:

$$\begin{cases} V_{panel} = \min_{j=1,\dots,p} (\sum_{i=1,\dots,s} V_{values,ij}) \\ I_{panel} = \sum_{j=1,\dots,p} (\min_{i=1,\dots,s} I_{values,ij}) \end{cases}$$

and $V_{values,ij}$ and $I_{values,ij}$ are the voltage and current extracted from the i -th PV module of the j -th string.

7.1.2 Connection with bypass diodes

When using diodes (i.e., $0 < d \leq N$), poorly irradiated modules of a series-connected string get bypassed and does not constrain anymore the current of the other ones: when the current gets larger than the maximum value that can be produced by the weakest module, the diode becomes forward biased and only the highly irradiated modules produce power [55]. Considering for simplicity the case of two modules with high (H) and low (L) irradiance, the total curve is therefore obtained by summing the I-V curves. For each current value in the range $[0, I_{SC,H}]$ the voltage is:

$$\begin{cases} V_{string} = V_L + V_H & \text{if } I < I_{SC,L} \\ V_{string} = V_H - V_d & \text{if } I_{SC,L} < I < I_{SC,H} \end{cases} \quad (11)$$

where $V_d = 0.6V$ is the voltage drop across a forward-biased diode. This yields the classical I-V curve with multiple “steps”, as shown in Figure 7.a.

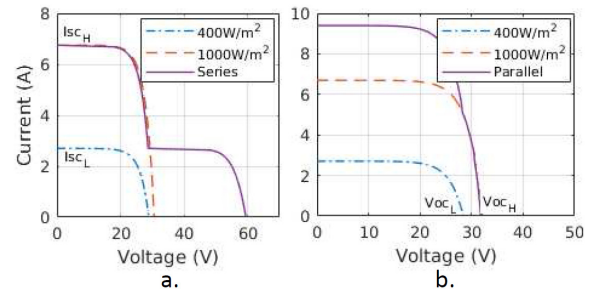


Fig. 7. I-V curves of the series (a) and parallel (b) connection of two modules with different G values with bypass diodes.

The result of combining the I-V curves in parallel is obtained by summing the current of the two modules for each voltage value in the range $[0, V_{OC,H}]$ as follows (Figure 7.b):

$$\begin{cases} I_{panel} = I_L + I_H & \text{if } V < V_{OC,L} \\ I_{panel} = I_H & \text{if } V_{OC,L} < V < V_{OC,H} \end{cases} \quad (12)$$

8 PLACEMENT CONFIGURATOR

The goal of the *Placement Configurator* block is to place the N PV modules in the area of interest. This block takes in input the topology information, the suitable area and the traces

produced by the *Trace Builder* block. Typical state-of-the-art frameworks take the placement in input, usually assuming a compact placement of PV modules on a delimited area of the roof. On the other hand, the evolution of shadows is crucial to ensure effective power production [15], as it can heavily impact the efficiency of the PV power production dynamics. For this reason, the framework includes a block devoted to placement, to compare the effect of different placements of PV modules on the roof and of different connections.

This component provides two built-in placement algorithms: one for building a traditional compact placement of panels (Figure 8.a), and the other optimized with respect to the distribution of G over the area (Figure 8.b, where darker areas are the least irradiated). Thanks to the microservices architecture, additional placement strategies can be included in our framework without affecting other blocks. The calculation of an optimum placement is unfeasible as it would require an exhaustive enumeration of all possible grid points, which becomes quickly intractable even for small areas [15]. It is also not possible to introduce bounds on the enumeration because the total extracted power can be computed only when all the modules are placed. Thus, the placement algorithms must necessarily follow some heuristic.

The resulting placement is then written in the JSON document, listing the left-top corner and the direction of each PV module, ordered so that the first s modules in the list represent one series-connected string.

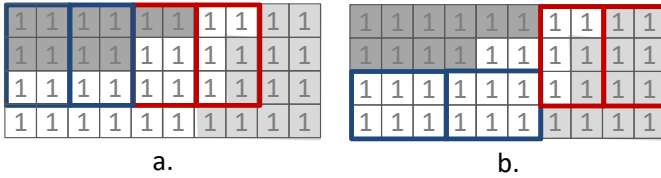


Fig. 8. Application of the compact placement (a) and of the optimized placement (b) to an example of roof with heterogeneous irradiance distribution. Darker cells are less irradiated. Rectangles represent PV modules, and rectangles of the same color belong to the same string.

8.1 Built-in Compact Placement Algorithm

The compact placement algorithm reproduces the traditional placement where PV modules are packed, as shown by Figure 8.a. This placement takes in input the coordinates of a cell, that is considered the left-top corner of the first PV module ((1, 1) in the example). Then, it tries to place the PV modules one close to the other, if necessary dividing the sequence in different rows. PV modules are then connected in series and parallel based on their spatial proximity (i.e., the first s PV modules form the first series string). It is easy to see that the complexity of this algorithm is $O(H \cdot W)$, as it involves similar operations to the feasibility check in the topology builder.

8.2 Built-in Optimized Placement Algorithm

The built-in optimized algorithm is a simple and efficient greedy solution: the algorithm allocates PV modules greedily, by trying to match the distribution of irradiance on the roof, as shown in Figure 8 (clearer cells are more irradiated).

8.2.1 Key idea of the algorithm

The starting point of the algorithm is the suitable area that is aligned with a virtual grid. As explained in Section 4, this allows to have traces of temperature and irradiance per each grid element over time, and thus to reason about the characteristics of the different portions of the roof. Note that the size of grid elements is chosen so that it is a divisor of the sizes of a PV module, so that each PV module occupies an integer number of grid elements. The problem is thus reduced to identifying which grid elements are occupied by each of the PV modules to be placed.

The choice of the position of each PV module is based on the construction of a suitability metric, that ranks roof locations according to their estimated effectiveness in terms of power generation. PV modules will thus be placed greedily in the more promising locations, according to the defined metric.

8.2.2 Definition of the suitability metric

PV power production is mostly affected by irradiance: over a range of $[200 - 1000] W/cm^2$, power changes by $5\times$, whereas typical T_{solair} ranges only change power by $\pm 20\%$ at most (see Figure 5). Thus, the suitability metric should be a proxy of irradiance, while temperature can be used as a corrective factor.

Additionally, the metric should distill the temporal traces into a compact signature. The instantaneous value of irradiance over time will indeed naturally vary, as an effect of sun movement in the sky. The metric should thus not consider the instantaneous value of irradiance, but rather a representative value of its global evolution.

The average is not a good choice because the typical distributions of irradiance and temperature are strongly skewed towards smaller values. We thus use the 75-th percentile of the distribution, i.e., the value below which 75% of the samples fall. Larger values of the percentile identify distributions that are more skewed towards the upper range of the values. Temperature is used as a corrective factor $f(T_{solair})$ that tracks the dP_{max}/dT as in middle plot of Figure 5.

The suitability s_{ij} of a grid cell (i, j) is thus obtained as $s_{ij} = p_{75}^{G_{ij}} \cdot f(T_{solair})$, where $p_{75}^{G_{ij}}$ is the 75-th percentile of G in the grid cell located at row i and column j .

It is important to note that a PV module does occupy more than one grid cell, and that the grid cell with the lowest irradiance determines the operating point of the whole module. To take this into account, before calculating the suitability metric, it is necessary to determine a modified trace of G values, where the G value at each time step evaluates to the minimum value of G among all “covered” grid cells.

8.2.3 Optimized placement algorithm

Figure 9 shows a pseudo-code of the algorithm.

First (Lines 1-3) the suitability matrix S is computed as described above by for each position of a PV module (i, j) and for both its portrait or landscape direction d . In Line 4, the grid coordinates and orientations (i, j, d) are sorted in an array L in decreasing order of their value of S . In case of identical values of suitability, the distance from the already placed modules is used as a tie-breaker, to account for the higher wiring cost (closer grid points have higher rank).

Inputs:

- **suitableArea** : suitable area for the PV installation
- **N, s, p**: topology of the PV installation
- **G[i,j,t], T[i,j,t]**: G and T vales for each grid cell $i=1,..., W$, $j=1,..., H$, and time t

Outputs:

- **Placement**: array of **N** coordinates **(i,j,d)** representing for each PV module its placement **(i,j)** and its orientation **d** (portray/landscape)

Algorithm:

```

1. for each cell (i,j) of the suitableArea
2.   Calculate the suitability metric S[i,j,d] (both portray and landscape)
3. endfor
4. L = array of cells with orientation (i,j,d) sorted in non-decreasing order of suitability (wiring overhead is used as a tie-breaker)
5. k=1
6. for each module m=1,..., N
7.   Placement[m]  $\leftarrow$  L[k]
8.   remove from S the grid cells "covered" by L[k] (landscape or portray)
9.   k  $\leftarrow$  k+1
10. endfor
11. return Placement

```

Fig. 9. Pseudocode of the optimized placement algorithm in Section 8.2.

We then iterate (Lines 6-10) over the N modules: the k -th module is placed in the m -th position according to the previously computed ranking (Line 7). Since a PV module occupies a number of grid cells, all these "covered" cells are clearly unusable and must therefore be removed from **L** (Line 8), depending on the orientation of the PV module. The algorithm marks as unusable also any grid cell that is not surrounded anymore by enough free grid cells to host a panel. We then pick the next coordinate from **L** after the removal of covered points. The loop terminates when the N modules have been placed. In this case, the time complexity of the placement is $O(H \cdot W \cdot Ts)$, where Ts is the number of samples in the G and T traces. In fact, it can be seen that the most complex step is the evaluation of the suitability metric, which requires processing the entire trace corresponding to each grid cell once.

9 POWER PRODUCTION ESTIMATOR

The *Power Production Estimator* block estimates the power production of the PV installation, given the placement of PV modules, their connection and the traces of G and T_{solair} over time. It is a relatively straightforward component implementing a trace-based simulation engine. At each time step, it derives the I-V curve of each PV module, given the placement of the PV module and the input traces. The I-V curves are derived by using either the function generated by the *PV Module Model Builder* block (Section 6) or a user-defined function. The I-V curves of all PV modules are then combined through the formulas presented in Section 7, that apply the series-parallel topology of PV modules to derive the resulting operating point of the overall PV panel, in terms of operating voltage, current and power. The estimator has time complexity $O(N \cdot Ts)$ as it involves the processing of the entire time series of G and T for each module in the panel. Note that the granularity of the input traces

can be tuned by the user, thus allowing different trade-offs in terms of computational complexity and output accuracy. The outputs of this service are the traces of power, voltage and current over time, corresponding to the operating point of the overall PV installation. These traces are saved as a JSON document.

10 SIMULATION RESULTS

In order to demonstrate the effectiveness of the proposed framework, we present two case studies with very different objectives and that use different features of the framework.

10.1 Choice of suitable PV module

The first scenario focuses on the choice of the most suitable PV module, given a fixed placement and topology.

10.1.1 Target of the case study

As a case study, we selected a building rooftop in our university campus in Turin, Italy. The DSM has a resolution of $0.25m^2$ and has been provided by the city council. Meteorological data (i.e. solar radiation and air temperature) are retrieved, through third-party web services, by a weather station in our campus as well. The weather station collects global horizontal radiation by a first class pyranometer that samples every minute. Then, these samples are averaged and provided every 15 minutes. The roof of interest is oriented towards S-W with inclination 27° . Its suitable area is $\approx 5.4 \times 15.8m$ (represented by the black area in Figure 10.a). The roof is subject to quite heterogeneous irradiance, caused by the neighbouring buildings projecting their shadows on different portions of the roof at different times of the day. The settings of the PV installation and the placement of the PV modules on the roof are fixed: the user aims at installing 16 PV modules in the colored area in Figure 10.a. The goal of this case study is to compare the installation of two alternative PV modules: the Mistubishi PV-MF165EB3 PV module [57] and the SunPower 225 PV module [58] (Table 2). The two PV modules are comparable in size ($\approx 80 \times 160cm$) and cost. However, from Table 2 it is evident that the rated power is much higher for the SunPower PV module than for the Mistubishi one: the former may thus seem an optimal cost/production tradeoff ($\text{€}2.1/W$ versus $\text{€}2.5/W$).

TABLE 2
Characteristics of the compared PV modules

PV module	Rated (W)	Cost (€)	Yearly (MWh)	Cells (#)	Diodes (#)
Mistubishi PV-MF165EB3	165	412.50	3.37	5×10	5
SunPower 225	225	472.50	2.46	12×6	3

10.1.2 Adoption of the proposed framework

To compare the two PV modules at work, we configured the framework as follows. The *PV Module Model Builder* is run twice on the input specifications of the two PV modules, i.e., their datasheet curves, to fit the equations in Section 6 to the characteristics of the two PV modules. The configuration of the PV installation in terms of number of PV modules

and their topology is given by the user, thus the *Topology Builder* block is not executed, and it is replaced with an input custom topology of 8×2 . The topology is used by the *PV Panel Model Builder* to reconstruct operation over time of the overall PV installation from the individual contribution of PV modules. The *Placement Configurator* block is run to obtain the desired compact placement (Figure 10.a, where rectangles with the same color are PV modules connected in series). Finally, we used the *Simulator* block to launch a 1-year long simulation by using environmental traces referred to the year 2013, elaborated from meteorological data collected by a nearby weather station ($< 1\text{km}$) by the *Trace Builder* block.

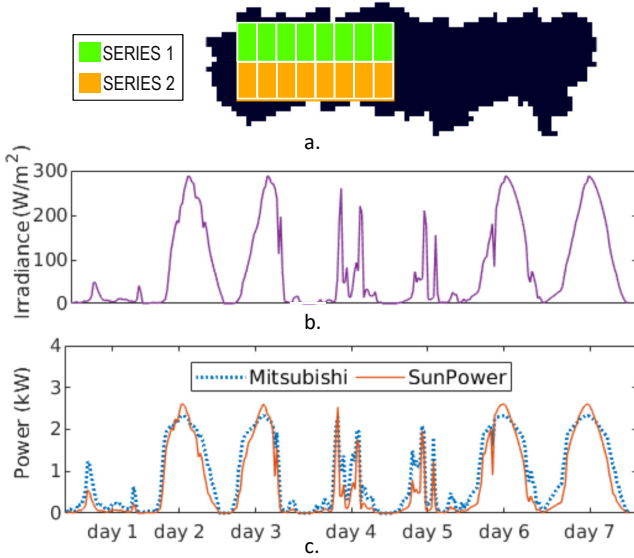


Fig. 10. Scenario 1: (a) placement of PV modules (PV modules of the same color belong to the same series string), (b) average irradiance over the roof over one week, and (c) estimated power production for the Mitsubishi PV-MF165EB3 PV module (dashed) and the SunPower 225 PV module (solid).

10.1.3 Outcome of framework adoption

After framework execution, we analysed the output of the *Simulator* block. Figure 10b-c shows a zoom-in on one week: average irradiance over the roof (b) and power production of the PV installations (c). Interestingly, the simulation reveals that the PV module with the lowest rated power (i.e., the Mistubishi one) achieves a higher yearly power production by +36.68%. This is easily explained by looking at Figure 10.c: the SunPower modules perform better during the peaks, i.e., around midday, when irradiance is evenly distributed over the roof. Vice versa, at times of the day when shadows are more consistent (i.e., morning and afternoon) the Mistubishi modules show a better resilience to partial shading. This is due to the different technology (i.e., polycrystalline vs. monocrystalline) [59] and to the different diode distribution inside of each PV module: the SunPower PV module contains 3 diodes, each controlling 24 cells, while the Mistubishi one contains 5 diodes, one every 10 cells. This ensures a finer granularity in the management of partial shading for the Mitsubishi PV module.

10.1.4 Effectiveness of the proposed framework

The framework allowed to compare the two PV modules over real environmental traces and to make a more in-

formed choice of the best candidate: the cheapest PV module (i.e., the Mistubishi one) proved indeed to ensure a higher power production with the typical yearly varying weather conditions. This result has been achieved by invoking the different services of the framework, and information has been managed with no manual intervention other than providing input settings.

The approaches listed in Section 2.3 would not allow such a detailed analysis of the case study. First of all, the scenario requires high resolution data, to reproduce the evolution of shadows over the day on small portions of the roof. Additionally, only a detailed model of PV production allows to capture the different behavior of the PV modules under analysis: a model restricted to the power dependence on occupied area or on rated power would not allow to capture the difference in terms of power production under heterogeneous shadow distribution.

10.2 Choice of most effective placement of PV modules

The second scenario focuses on an exploration of different placements of the PV modules.

10.2.1 Target of the case study

The roof of interest is a lean-to roof of an industrial building, with a suitable area of $30.8 \times 10.2\text{m}$, facing S/S-W with inclination of 26° . As evident from Figure 11.a, the irradiance is unevenly distributed over the roof, with encumbrances and neighboring buildings that project shadows mostly on the right-hand side. The goal of this case study is thus to identify an effective placement of PV modules so to maximize power production with economic constraints. The chosen PV module is the Mistubishi PV-MF165EB3 PV module [57].

10.2.2 Adoption of the proposed framework

To design the target PV installation, we adopted the framework as follows. The *Topology Builder* block is used to determine the optimal topology: given an investment of 14k€ and a target voltage of 180V (settings provided as input configuration), the determined output topology is 6×6 . The installation will thus feature 36 Mistubishi PV-MF165EB3 PV modules. The *PV Module Model Builder* block and the *PV Panel Model Builder* are used to estimate power production, given the Mistubishi PV-MF165EB3 PV module specifications and the derived topology. The *Placement Configurator* block is executed twice to obtain an optimal placement and a compact placement. Figure 11 shows roof configuration (a) and the two placements (b and c, respectively). Both placements fall on the left-hand side of the roof, that is more irradiated. The optimal placement is sparser as it tries to exploit fine-grain differences in the distribution of G and T, e.g., by maximizing the presence of PV modules in the most irradiated area. Note that the user may investigate the effect of a placement on the right hand side of the roof by changing the initial point of the compact placement, or by restricting the suitable area used by the optimal placement. However, any placement in this portion of the roof would be sub-optimal, given the uneven distribution of irradiance. To compare the two placements, we used the *Simulator* block to launch a 1-year long simulation by using the same data of the previous experiment, derived by the *Trace Builder* block.

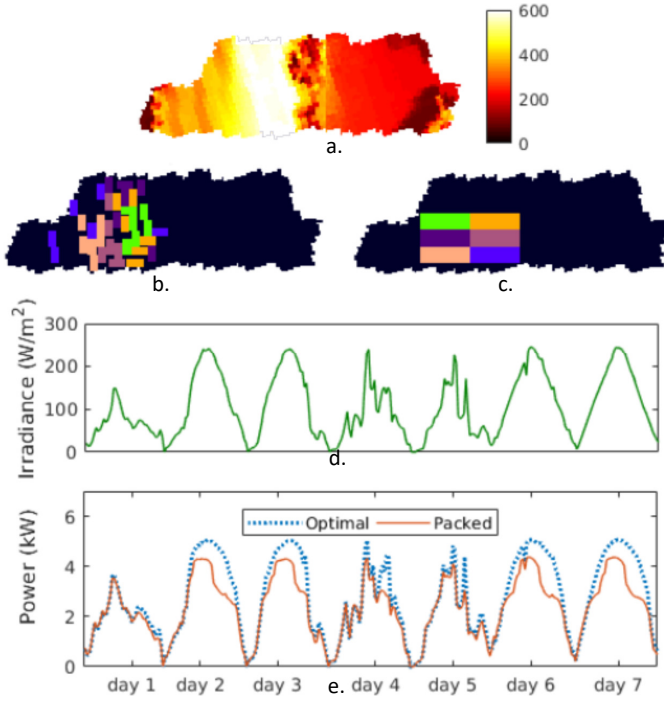


Fig. 11. Scenario 2: (a) 75th percentile of irradiance over the roof represented as a heatmap, (b) optimized placement, (c) compact placement, (d) average irradiance over the roof for one week, and (e) estimated power production for the two placements.

10.2.3 Outcome of framework adoption

After simulation, we analyzed the output of the *Simulator* block. Figure 10d-e show a zoom into one week, by showing the average irradiance over the roof and the corresponding power output of the PV installation (dashed for the optimal placement, solid for the compact one). It is evident that the optimal placement achieves higher power production given the same irradiance conditions. This is due to two main factors. First, PV modules are placed in the most irradiated areas, while the compact placement occupies also less irradiated portions of the roof.

Another crucial aspects that impacts on the output power production is the connection of PV modules to realize the 6×6 topology (in Figure 10b-c, rectangles with the same color are PV modules connected in series). The compact placement connects in series PV modules based on spatial proximity, while the optimal placement connects in series PV modules with similar irradiance conditions, thus minimizing the bottleneck effect.

The result is that the optimal placement achieves +19.48% yearly power production (i.e., 10.372MWh vs. 8.681MWh). This proves the superiority of the greedy placement approach over a standard rule-of-thumb compact placement.

10.2.4 Effectiveness of the proposed framework

The framework allowed to compare two PV installations with the same number and type of PV modules and with the same topology, but different in terms of PV module placement and connection. This experiment proves that the flexibility offered by microservices to extend and compare different versions of the same block (e.g., different placement algorithms) enhances design space exploration and

allows to identify more optimized configurations for the target PV installation.

This experiment would be unfeasible with the approaches listed in Section 2.3: it requires indeed not only high resolution of data, but also a detailed modeling of the placement of PV modules in the area of interest. Thus, all works operating on large areas or fixed placements are not applicable to this scenario. Additionally, the different behavior with heterogeneous irradiance distribution on the roof can be appreciated only with detailed models of PV production, with awareness of the presence of diodes and of the connection between PV modules.

11 CONCLUSIONS

The paper presented a framework to improve the effectiveness of PV installation design. The framework is built as a set of microservices, that provide built-in implementations and that support multiple scenarios and user customization. The paper discussed the effectiveness of the framework with two scenarios, focusing on two different roofs and, more importantly, on two different usage flows of the framework. These case studies allowed to highlight the impact of the proposed framework on PV installation design, i.e., in the placement of PV modules and in the choice of PV module to buy, thus sensibly improving installation design.

REFERENCES

- [1] N. M. Pearsall, "PV research and development in Europe – a view from the technology platform," in *IEEE PVSC*, 2011, pp. 200–205.
- [2] Y. Ghiassi-Farrokhfal, F. Kazhamiaki, C. Rosenberg, and S. Keshav, "Optimal design of solar pv farms with storage," *IEEE Transactions on Sustainable Energy*, vol. 6, no. 4, pp. 1586–1593, 2015.
- [3] W. Khemiri, R. Yaagoubi, and Y. Miky, "Optimal placement of solar photovoltaic farms using analytical hierarchical process and geographic information system in mekkah, saudi arabia," in *AIP Conference Proceedings*, vol. 2056, 2018, pp. 1–10.
- [4] N. Lukač, D. Špelič, G. Štumberger, and B. Žalik, "Optimisation for large-scale photovoltaic arrays – placement based on light detection and ranging data," *Applied Energy*, vol. 263, p. 114592, 2020.
- [5] I. Gašparović and M. Gašparović, "Determining optimal solar power plant locations based on remote sensing and gis methods: A case study from croatia," *Remote Sensing*, vol. 11, no. 12, p. 1481, 2019.
- [6] P. Phonrattanasak, M. Miyatake, and O. Sakamoto, "Optimal location and sizing of solar farm on japan east power system using multiobjective bees algorithm," in *2013 IEEE Energytech*, 2013, pp. 1–6.
- [7] M. Y. Khan, M. Ali, S. Qaisar, M. Naeem, C. Chrysostomou, and M. Iqbal, "Placement optimization for renewable energy sources: Ontology, tools, and wake models," *IEEE Access*, vol. 8, pp. 72 781–72 800, 2020.
- [8] C. Keerthisinghe, G. Verbic, and A. C. Chapman, "Evaluation of a multi-stage stochastic optimisation framework for energy management of residential PV-storage systems," in *IEEE AUPEC*, 2014, pp. 1–6.
- [9] R. Atia and N. Yamada, "Sizing and analysis of renewable energy and battery systems in residential microgrids," *IEEE Transactions on Smart Grid*, vol. 7, no. 3, pp. 1204–1213, 2016.
- [10] F. Luo, G. Ranzi, C. Wan, Z. Xu, and Z. Y. Dong, "A multistage home energy management system with residential photovoltaic penetration," *IEEE TII*, vol. 15, no. 1, pp. 116–126, 2019.
- [11] M. Aghamohamadi, A. Mahmoudi, and M. Haque, "Two-stage robust sizing and operation co-optimization for residential pv-battery systems considering the uncertainty of pv generation and load," *IEEE Transactions on Industrial Informatics*, pp. 1–1, 2020.

- [12] Y. Chen, D. Jahier Pagliari, E. Macii, and M. Poncino, "Battery-aware design exploration of scheduling policies for multi-sensor devices," in *Proceedings of the 2018 on Great Lakes Symposium on VLSI*, ser. GLSVLSI, 2018, p. 201. doi:10.1109/GLSVLSI.2018.8420606.
- [13] A. Goodrich, T. James, and M. Woodhouse, "Residential, commercial, and utility-scale photovoltaic (PV) system prices in the united states: Current drivers and cost-reduction opportunities," <https://www.nrel.gov/docs/fy12osti/53347.pdf>, pp. 1–64, 2012.
- [14] T. Voegtli, E. Steinle, and D. Tóvári, "Airborne laserscanning data for determination of suitable areas for photovoltaics," in *ISPRS LS*, 2005.
- [15] S. Vinco, L. Bottaccioli, E. Patti, A. Acquaviva, E. Macii, and M. Poncino, "GIS-based optimal photovoltaic panel floorplanning for residential installations," *IEEE DATE*, 2018.
- [16] S. Vinco, E. Macii, and M. Poncino, "Optimal topology-aware PV panel floorplanning with hybrid orientation," in *GLS-VLSI*, 2018, pp. 491–494.
- [17] M. Severini, A. Scorrano, S. Squartini, M. Fagiani, and F. Piazza, "SW framework for simulation and evaluation of partial shading effects in configurable PV systems," in *IEEE EEEIC*, 2016, pp. 1–6.
- [18] P. Manganiello, M. Baka, H. Goverde, T. Borgers, J. Govaerts, A. van der Heide, E. Voroshazi, and F. Catthoor, "A bottom-up energy simulation framework to accurately compare PV module topologies under non-uniform and dynamic operating conditions," in *IEEE PVSC*, 2017, pp. 3343–3347.
- [19] S. Kucuksari, A. M. Khaleghi, M. Hamidi, Y. Zhang, F. Szidarovszky, G. Bayraktan, and Y.-J. Son, "An integrated GIS, optimization and simulation framework for optimal PV size and location in campus area environments," *Applied Energy*, vol. 113, pp. 1601–1613, 2014.
- [20] M. Fowler and J. Lewis, "Microservices," 2019, <http://martinfowler.com/articles/microservices.html>.
- [21] G. Adinolfi, G. Graditi, P. Siano, and A. Piccolo, "Multiobjective optimal design of photovoltaic synchronous boost converters assessing efficiency, reliability, and cost savings," *IEEE TII*, vol. 11, no. 5, pp. 1038–1048, 2015.
- [22] B. Resch, G. Sagl, T. Törnros, A. Bachmaier, J.-B. Eggers, S. Herkel, S. Narmsara, and H. Gündra, "GIS-based planning and modeling for renewable energy: Challenges and future research avenues," *ISPRS IJGI*, vol. 3, no. 2, pp. 662–692, 2014.
- [23] Mapdwell Solar System. <http://www.mapdwell.com>.
- [24] L. de Sousa, C. Eykamp, U. Leopold, O. Baume, and C. Braun, "iguess-a web based system integrating urban energy planning and assessment modelling for multi-scale spatial decision making," in *iEMSs 2012*, 2012.
- [25] R. De Amicis, G. Conti, D. Patti, M. Ford, and P. Elisei, "I-scope-interoperable smart city services through an open platform for urban ecosystems," 2012, <http://www.iscopeproject.net>.
- [26] S. Ferlito, G. Adinolfi, and G. Graditi, "Parametric analysis and systems design of dynamic photovoltaic shading modules," *Energy Science and Engineering*, vol. 4, pp. 134–152, 2016.
- [27] M. Brumenm, N. Lukac, and B. Zalik, "GIS application for solar potential estimation on buildings roofs," in *IARIA WEB*, 2015.
- [28] B. Marion and M. Anderberg, "PVWATTS - an online performance calculator for grid-connected PV systems," in *ASES SOLAR*, 2000, pp. 119–124.
- [29] PVGIS. http://re.jrc.ec.europa.eu/pvg_tools/en/tools.html.
- [30] K. Mainzer, S. Killinger, R. McKenna, and W. Fichtner, "Assessment of rooftop photovoltaic potentials at the urban level using publicly available geodata and image recognition techniques," *Solar Energy*, vol. 155, pp. 561–573, 2017.
- [31] F. Kazhamiaka, Y. Ghiassi-Farrokhfal, S. Keshav, and C. Rosenberg, "Comparison of different approaches for solar PV and storage sizing," *IEEE TSUSC*, 2019.
- [32] A. K. Shukla, K. Sudhakar, and P. Baredar, "Design, simulation and economic analysis of standalone roof top solar pv system in india," *Solar Energy*, vol. 136, pp. 437–449, 2016.
- [33] S. Suman and S. De, "Low complexity dimensioning of sustainable solar-enabled systems: A case of base station," *IEEE TSUSC*, 2019.
- [34] X. Gong and M. Kulkarni, "Design optimization of a large scale rooftop photovoltaic system," *Solar Energy*, vol. 78, no. 3, pp. 362–374, 2005.
- [35] R. Rachchh, M. Kumar, and B. Tripathi, "Solar photovoltaic system design optimization by shading analysis to maximize energy generation from limited urban area," *Energy conversion and management*, vol. 115, pp. 244–252, 2016.
- [36] M. Oh and H.-D. Park, "Optimization of solar panel orientation considering temporal volatility and scenario-based photovoltaic potential: A case study in seoul national university," *Energies*, vol. 12, no. 17, p. 3262, 2019.
- [37] D. Sera, R. Teodorescu, and P. Rodriguez, "PV panel model based on datasheet values," in *Proc. of IEEE ISIE*, 2007, pp. 2392–2396.
- [38] M. G. Villalva, J. R. Gazoli, and E. R. Filho, "Comprehensive approach to modeling and simulation of photovoltaic arrays," *IEEE Transactions on Power Electronics*, vol. 24, no. 5, pp. 1198–1208, 2009.
- [39] S. Vinco, Y. Chen, E. Macii, and M. Poncino, "A unified model of power sources for the simulation of electrical energy systems," in *Proc. of ACM/IEEE GLSVLSI*, 2016, pp. 281–286.
- [40] R. S. Magdaleno, P. A. Sanchez-Perez, J. L. Z. Ramirez Cruz, D. M. Escobar, and A. Sánchez-Juarez, "Influence of partial shading on the power output of a solar cell and a pv module," in *Proc. of IEEE PVSC*, 2018, pp. 1324–1327.
- [41] S. Guo, T. M. Walsh, A. G. Aberle, and M. Peters, "Analysing partial shading of pv modules by circuit modelling," in *Proc. of IEEE PVSC*, 2012, pp. 2957–2960.
- [42] M. Udell and O. Toole, "Optimal design of efficient rooftop photovoltaic arrays," *Interfaces*, vol. 49, no. 4, pp. 281–294, 2019.
- [43] S. Ferlito, G. Adinolfi, and G. Graditi, "Comparative analysis of data-driven methods online and offline trained to the forecasting of grid-connected photovoltaic plant production," *Applied Energy*, vol. 205, pp. 116–129, 2017.
- [44] S. Newman, *Building Microservices*. O'Reilly Media, Inc., 2015.
- [45] R. T. Fielding and R. N. Taylor, "Principled design of the modern web architecture," *ACM TOIT*, vol. 2, no. 2, pp. 115–150, May 2002.
- [46] L. Bottaccioli, E. Patti, E. Macii, and A. Acquaviva, "GIS-based software infrastructure to model pv generation in fine-grained spatio-temporal domain," *IEEE Systems Journal*, 2017.
- [47] Open Source Geospatial Foundation, "Geographic resources analysis support system (GRASS GIS) software," <http://grass.osgeo.org>, 2015.
- [48] N. Engerer, "Minute resolution estimates of the diffuse fraction of global irradiance for S-E Australia," *Elsevier SE*, vol. 116, pp. 215–237, 2015.
- [49] L. R. Camargo, R. Zink, W. Dorner, and G. Stoeglehner, "Spatio-temporal modeling of roof-top photovoltaic panels for improved technical potential assessment and electricity peak load offsetting at the municipal scale," *Elsevier COMPENVURBSYS*, vol. 52, pp. 58–69, 2015.
- [50] A. Ahadi and X. Liang, "A stand-alone hybrid renewable energy system assessment using cost optimization method," in *IEEE ICIT*, 2017, pp. 376–381.
- [51] Mitsubishi Electric, "PV-MF165EB3 (165Wp)," <https://www.mitsubishielectricsolar.com>, 2004.
- [52] S. Vinco, L. Bottaccioli, E. Patti, A. Acquaviva, and M. Poncino, "A compact PV panel model for cyber-physical systems in smart cities," in *IEEE ISCAS*, 2018, pp. 1–5.
- [53] F. Brihmat and S. Mekhtoub, "PV cell temperature/PV power output relationships Homer methodology calculation," in *IJSET*, vol. 1, 2014.
- [54] A. M. Reis, N. T. Coleman, M. W. Marshall, P. A. Lehman, and C. E. Chamberlin, "Comparison of PV module performance before and after 11-years of field exposure," in *IEEE PVSC*, 2002, pp. 1432–1435.
- [55] A. Smets, K. Jager, O. Isabella, R. van Swaaij, and M. Zeman, *Solar Energy: The physics and engineering of photovoltaic conversion, technologies and systems*. UIT Cambridge, 2016.
- [56] Coulee Energy, "Blocking and bypass diodes in a solar system," <https://couleeenergy.com/bypass-diodes-in-solar-panels/>, 2019.
- [57] PV-MF165EB3 Datasheet, 2004, www.mitsubishielectricsolar.com.
- [58] 225 solar panel Datasheet, 2008, www.energymatters.com.au.
- [59] I. Faye, A. Ndiaye, D. Kobor, M. Thiame, C. Sene, and L.-G. Ndiaye, "Evaluation of the impact of partial shading and its transmittance on the performance of crystalline silicon photovoltaic modules," *Academic Journals*, vol. 12, no. 21, pp. 286–294, 2017.



Sara Vinco (M'09) is Assistant Professor at Politecnico di Torino, Turin, Italy. She received the Ms.C. and the Ph.D. degree in Computer Science from the University of Verona, Verona, Italy, in 2009 and 2013, respectively. Her current research interests include energy efficient electronic design automation, efficient simulation and optimization of energy systems, and techniques for simulation and validation of heterogeneous embedded systems.



Massimo Poncino (SM'12-F'18) is a Full Professor of Computer Engineering with the Politecnico di Torino, Torino, Italy. His current research interests include several aspects of design automation of digital systems, with emphasis on the modeling and optimization of energy-efficient systems. He received a PhD in computer engineering and a Dr.Eng. in electrical engineering from Politecnico di Torino. He is a Fellow of the IEEE.



Daniele Jahier Pagliari (M'15) received the M.Sc. and Ph.D. degrees in computer engineering from Politecnico di Torino, Torino, Italy, in 2014 and 2018, respectively. He is currently an Assistant Professor in the same institution. His research interests include computer-aided design of digital systems, with particular emphasis on low-power optimization and approximate computing.



Lorenzo Bottaccioli (M'15) is Assistant Professor at the Energy Center Lab of Politecnico di Torino (Italy). In 2018 received the PhD, cum laude, in Computer Engineering at Politecnico di Torino. His main research interests concern Smart Energy, Smart City and Smart Communities with focus on software solutions i) for planning, analysing and optimising smart energy system and ii) for spatial representation of energy information.



Edoardo Patti (M'16) is Assistant Professor at Politecnico di Torino. He received both M.Sc. and Ph.D. degrees in Computer Engineering at Politecnico di Torino in 2010 and 2014, respectively. His research interests concern: ubiquitous computing and Internet of Things; smart systems, cities and mobility; software architectures with particular emphasis on infrastructure for Ambient Intelligence; software solutions for simulating and optimising energy systems and for energy data visualisation to increase user awareness.



Enrico Macii (SM'02-F'05) is a Full Professor of Computer Engineering with the Politecnico di Torino, Torino, Italy. He holds a Laurea degree in electrical engineering from the Politecnico di Torino, a Laurea degree in computer science from the Università di Torino, Turin, and a PhD degree in computer engineering from the Politecnico di Torino. His research interests are in the design of electronic digital circuits and systems, with a particular emphasis on low-power consumption aspects. He is a Fellow of the IEEE.